FIRE RESISTANCE OF STEEL-CONCRETE SIDE-PLATED BEAMS

Jerneja Kolšek [a], Tomaž Hozjan [a], Miran Saje [a], Igor Planinc [a]

[a] University of Ljubljana, Faculty of Civil and Geodetic Engineering, Ljubljana, Slovenia

Abstract

In the paper a novel three-phase finite-element numerical model for the fire analysis of side-plated reinforced concrete (RC) beams is presented. In addition, advantages of beam side reinforcing as a measure of structural retrofitting are explored for a selected case and an important contribution of the side plates to the ultimate fire resistance of the RC beam is observed.

Keywords: side–plated beam, fire, longitudinal slip, transversal slip, moisture transfer, heat transfer, high temperatures.

INTRODUCTION

Over the course of the past few decades the technique of plating of flexural beams has become acknowledged as one of the peak engineering solutions of structural retrofitting. During this time a vast number of different plating solutions has been introduced in the market (i.e. the tension-face plating technique, the side-plating technique, the U wraps, etc.), yet it seems, that for every day engineering purposes only the tension face plating technique has been widely accepted. Undoubtedly, this is also a reflection of the current status of the scientific publications. While a vast number of favourable scientific findings have been presented in the field of the research of the tension face plated beams, the reports on the investigations of the alternatively plated beams are extremely rare and our understanding of their behaviour under different types of loading (especially such as in fire) is still poor.

When considering RC beams at high temperatures a complex numerical analysis cannot be avoided. To fully understand the complexity of the problem, the microscopic structure of concrete and changes, that it undergoes at high temperatures, need to be looked in detail. Concrete consists of not only the hardened cement paste but also of pores partially filled with water (liquid, adsorbed or chemically bound) and with the gaseous mixture of dry air and water vapour. Due to the presence of gas and water the heat capacity of the material is increased and, in addition, heat is not only conducted but also convected through the material and accompanied with chemical decomposition and phase changes (water evaporation and vapour condensation). On top of the temperature gradients, also the pressure and the concentration gradients are established inside the concrete body and free water and gas fluxes are evoked. Depending on the permeability of the thermally and mechanically damaged material, these are headed partially outwards, towards the heated surface, and partially inwards, towards the cooler layers of concrete where vapour condenses. Inside the concrete body, in the area where the permeability of the material is substantially diminished (e.g. due to high saturation levels), the gas and water flow is hindered and its speed is reduced. This (so called) plugged zone eventually causes a rapid rise of pore pressures in front of the zone, accelerated crack propagation in this area and, in most severe cases, explosive spalling (separation) of the damaged material.

Within the last decade, several different models have been suggested in scientific literature for analyses of concrete structures at high temperatures. Depending on whether ‘mechanical’ (stress induced) damage effects are accounted for in the heat and mass transfer inside the concrete element or not, two fundamental groups of such models can be distinguished. The first group represents the models (e.g., Davie et al., 2006), where the mechanical effects are

neglected in total. In line with this assumption, these models are only applicable for concrete structures with zero mechanical loading and where thermal dilatations of the concrete element are not (significantly) restrained, so that no (significant) stress is induced in the element during fire. For a general case of a mechanically loaded concrete structure in fire, however, only the alternative fully coupled thermo-hygro-mechanical models are commonly applicable (e.g. Gawin et al., 2003). Unfortunately, in these sophisticated models, extremely complex systems of governing equations and their respective constitutive relationships are usually observed and the accompanying numerical procedures are often found as unmanageably time consuming. As a result, the applicability of these models for different types of concrete and composite concrete structures is still limited and only specific problems with a small number of DOFs are mostly analysed in this way. In lieu of complex hydro-thermo-mechanical models, therefore, an empirically validated proposal for capturing the 'mechanical' effects in a pure hygro-thermal model indirectly has been recently presented by Dwaikat and Kodur (2010).

In the present paper a new three-phase numerical model for thermo-mechanically loaded side–plated RC beams is presented. In the first phase of the model, the time-dependent change of temperatures in the fire compartment surrounding the structure is defined, e.g. by engaging a CFD model of fire–driven fluid flows or by selecting an adequate fire curve prescribed in standards and regulations. For the sake of simplicity, the standard ISO 834 fire curve is engaged in this paper. The following hygro-thermal phase of the model is based on the model of Davie et al. (2006). Within the latter the proposal of Dwaikat and Kodur (2010) is additionally implemented capturing the effects of mechanical damage of concrete on its time-dependent permeability. Such combined model accounts for: (i) the porous and multiphase nature of concrete, (ii) phase and chemical transformations, and (iii) mutual interactions and couplings between the thermal, hygral and (indirectly) mechanical degradation of concrete. For the final, mechanical, part of the analysis, a new mathematical model and a strain-based FE formulation is proposed by the authors. In this part of the model the following phenomena are considered: (iv) partial longitudinal and transversal interlayer interaction, (v) stress-induced viscous creep of steel, and (vi) stress-induced creep and transient deformations of concrete. In zones where due to the changes in temperatures cyclic loading and reloading of the material is triggered, (vii) elastic reloading and (viii) kinematic hardening of the material are assumed. Since the separate phases of the proposed model have already been extensively validated against experiments elsewhere (see, e.g. Kolšek, 2013), this part of the presentation of the model is in the paper omitted. The paper concludes with a case study exploring the effects of the side strengthening of a selected RC beam on its fire resistance.

1 THERMO-HYGRO-MECHANICAL ANALYSIS OF A SIDE-PLATED RC BEAM

In this paper, firstly, for the description of the time development of temperatures of the fire compartment surrounding the side-plated beam, the standard ISO 834 fire curve is selected. Secondly, the coupled heat and mass transfer in the beam is observed and, thirdly, the mechanical response of the structure during fire is pursued. For the second and the third phase of the model two mathematically independent submodels are suggested. Within each, the total duration time of the fire is divided into time intervals $[t^{j-1}, t^{j}]$, and for each of the intervals the basic unknowns of the problem are iteratively determined.

1.1 The heat and mass transfer submodel

In the second phase of the proposed model the time and space distributions of temperatures and pore pressures in the side-plated RC beam are determined. For the non-porous side plates Fourier law of heat conduction is employed. For the heterogeneous RC beam the model of Davie et al. (2006) is selected comprising three governing equations of mass conservation of free water, water vapour and dry air:

$$\frac{\partial\left(\overline{\rho_{FW}}\right)}{\partial t} = -\nabla \mathbf{J}_{FW} - \dot{E}_{FW} + \frac{\partial\left(\overline{\rho_D}\right)}{\partial t},$$
$$\frac{\partial\left(\overline{\rho_V}\right)}{\partial t} = -\nabla \mathbf{J}_V + \dot{E}_{FW}, \tag{1}$$
$$\frac{\partial\left(\overline{\rho_A}\right)}{\partial t} = -\nabla \mathbf{J}_A,$$

and the governing equation of energy conservation:

$$\left(\underline{\rho C}\right)\frac{\partial T}{\partial t} = -\nabla\cdot\left(-k\nabla T\right) - \left(\underline{\rho C \mathbf{v}}\right)\cdot\nabla T - \lambda_E \dot{E}_{FW} - \lambda_D \frac{\partial\left(\overline{\rho_D}\right)}{\partial t}. \tag{2}$$

In Eqs. (1)–(2), $\mathbf{J}_i$ is the mass flux of phase i, $\overline{\rho_i}$ is the mass concentration of phase i, $\dot{E}_{FW}$ the rate of evaporation of free water (including desorption), and t is time. Index i denotes phases of concrete: FW is free water, V is water vapour and A is dry air. In Eq. (2) $\underline{\rho C}$ is heat capacity of concrete, k is its thermal conductivity, $\underline{\rho C \mathbf{v}}$ relates to the energy transferred by fluid flow, λ_E is the specific heat of evaporation, λ_D specific heat of dehydration and T is temperature.

The mass fluxes $\mathbf{J}_i$ are further expressed in terms of pressure and concentration gradients assuming that the Darcy's and Fick's laws are applicable. These and all of the other respective constitutive equations are in the model adopted as proposed by Davie et al. (2006), thus, they are not presented in this paper. Nevertheless, an exception regarding the time dependent concrete permeability evaluations is suggested. In contrast to case studies of Davie et al. (2006) dealing with problems, where zero 'mechanical' effects in the pressure-driven flow evaluations were assumed, such an assumption is no longer valid when a general case of a fire exposed side-plated RC beam is analysed. Instead, the 'mechanical' effects need to be explicitly considered. Indirectly, as recently proposed by Dwaikat and Kodur (2010), this can be performed by accounting for the gradients in the initial permeability of concrete, k_0:

$$k_0 = k_{top}\begin{Bmatrix} 10^{2y/D} & y \le x \\ 10^{2y/D}\left(10^{3(y-x)/(D-x)}\right) & y > x \end{Bmatrix}. \tag{3}$$

In Eq. (3) k_{top} refers to initial permeability in the top surface of the concrete section, D to the depth of the concrete cross-section, y is the distance from top of the cross-section, and x is the depth of neutral axis at service load and ambient temperature. Further, at each time station $t > 0$, the permeability of concrete, k, is evaluated in dependency on temperature, T, and the averaged pressure of liquids and gas inside the solid concrete matrix (i.e. pore pressure), P_{pore} (Dwaikat and Kodur, 2010, Gawin et al., 2002):

$$k = k_0\left[10^{0.0025(T-T_0)}\left(\frac{P_{pore}}{P_0}\right)^{0.368}\right]. \tag{4}$$

The solution of the presented hygro-thermal submodel is finally obtained numerically with the Galerkin's type of the finite element method as proposed in Davie et al. (2006).

1.3 The stress-strain evolution submodel

Once the temperature and pore pressure variation in time and space has been obtained, the stress-strain state evolution in the beam during fire can be pursued. In the mechanical submodel both of the layers of the steel–concrete side-plated beam (i.e. the layer '*a*' representing the RC beam and the layer '*b*' representing the side plates) are modelled

separately, each by the geometrically exact theory of a planar beam but neglecting the effects of shear deformations. The related governing equations of the layer '*i* ' (*i* = *a,b*) are:

- kinematic:
- equilibrium:
- constitutive:

$$
\begin{aligned}
&1+u^{i}{}'-\left(1+\varepsilon^{i}\right)\cos\varphi^{i}=0, && R_X^{i}{}'+\mathscr{P}_X^{i}=0, && N^{i}=\int_{\mathscr{A}_x^{i}}\sigma^{i}\left(D_\sigma^{i},T\right)dA-N_p^{i},\\
&w^{i}{}'+\left(1+\varepsilon^{i}\right)\sin\varphi^{i}=0, && R_Z^{i}{}'+\mathscr{P}_Z^{i}=0, && \\
&\varphi^{i}{}'-\kappa^{i}=0 && M^{i}{}'-\left(1+\varepsilon^{i}\right)Q^{i}+\mathscr{M}_Y^{i}=0, && M^{i}=\int_{\mathscr{A}^{i}}z\sigma^{i}\left(D_\sigma^{i},T\right)dA-M_p^{i}.
\end{aligned}
\qquad (5)
$$

(-)' in Eqs. (5) denotes the derivative with respect to material coordinate *x*. u^i, w^i and φ^i represent, respectively, the *X*-displacement, the *Z*-displacement and the rotation of the reference axis of the layer '*i*' and ε^i and κ^i are its extensional and bending strains (the curvature). R_X^i and R_Z^i are the components of the cross-sectional stress-resultants with respect to the fixed basis ($\boldsymbol{E}_X$, $\boldsymbol{E}_Y$, $\boldsymbol{E}_Z$) and N^i, Q^i, and M^i are the cross-sectional axial force, the shear force and the bending moment. Note, that R_X^i and R_Z^i relate to N^i and Q^i as follows: $N^i = R_X^i \cos\varphi^i - R_Z^i \sin\varphi^i$ and $Q^i = R_X^i \sin\varphi^i + R_Z^i \cos\varphi^i$ · Moreover, $\mathscr{P}_x^i$, $\mathscr{P}_z^i$, $\mathscr{M}_y^i$ denote components of the traction vectors $\boldsymbol{\mathscr{P}}^i$ and $\boldsymbol{\mathscr{M}}^i$ representing static equivalents of surface and volume forces after being reduced to the layer's reference axis, and N_p^i and M_p^i are the contributions of pore pressures in the total stress of the layer '*i*' (the well-known Terzaghi's principle). These are equal to zero when the non-porous steel side plates are considered (i.e. for *i* = *b*). Furthermore, σ^i and $D^i{}_\sigma$ are, respectively, stress and mechanical strain of a generic particle of the layer '*i*', and the relationship $\sigma^i(D^i{}_\sigma, T)$ is the material constitutive relationship of concrete/steel at elevated temperatures accounting also for elastic reloading and kinematic hardening of cyclically loaded and reloaded material. Based on the temperature of the time interval *j*, already determined within the hygro-thermal subanalysis, and the given stress and strain state in the time interval *j-1*, the mechanical strain of a generic particle, $D^{i,j}{}_\sigma$, is determined using the incremental equation:

$$D^{i,j} = D^{i,j-1} + \Delta D^{i,j}. \qquad (7)$$

In Eq. (7) $D^{i,j}$ is the increment of the total strain of the layer 'i' in the time interval *j*. Considering the principle of additivity of strains we assume that the strain increment, $\Delta D^{i,j}$, is the sum of the strain increments due to temperature, $\Delta D^i{}_{th}$, stress, $\Delta D^i{}_\sigma$, creep, $\Delta D^i{}_{cr}$, and (for concrete only) transient strains, $\Delta D^i{}_{tr}$ (with $\Delta D^a{}_{tr} \neq 0$ and $\Delta D^b{}_{tr} = 0$):

$$\Delta D^{i,j} = \Delta D_{th}^{i,j} + \Delta D_{\sigma}^{i,j} + \Delta D_{cr}^{i,j} + \Delta D_{tr}^{i,j}. \qquad (8)$$

By decomposing the traction (load) vectors of both layers with respect to their external (index 'e') and the contact (index 'c') contributions:

$$\boldsymbol{\mathscr{P}}^i = \boldsymbol{\mathscr{P}}_e^i \pm \boldsymbol{\mathscr{P}}_c^i \quad \text{and} \quad \boldsymbol{\mathscr{M}}^i = \boldsymbol{\mathscr{M}}_e^i \pm \boldsymbol{\mathscr{M}}_c^i, \qquad (6)$$

the equations of the side plates and the equations of the beam are finally coupled. The contact contributions, $\boldsymbol{\mathscr{P}}_c^i$ and $\boldsymbol{\mathscr{M}}_c^i$ (where $\boldsymbol{\mathscr{P}}_c^a = -\boldsymbol{\mathscr{P}}_c^b$ and $\boldsymbol{\mathscr{M}}_c^a = -\boldsymbol{\mathscr{M}}_c^b$), depend on the longitudinal (ΔU) and transversal (ΔW) slips between the layers, i.e. $\boldsymbol{\mathscr{P}}_c^i = f(\Delta U, \Delta W)$ and $\boldsymbol{\mathscr{M}}_c^i = g(\Delta U, \Delta W)$, where *f* and *g* are functions determined by experiments for the actual type of the contact connection.

Based on the modified principle of virtual work, the final system of equations of the mechanical submodel, briefly presented above, is finally solved by a novel strain-based FE method. For a detailed description of the proposed mechanical submodel, its governing as

well as its auxiliary equations and the numerical solving procedure a reader is referred to Kolšek et al. (2013).

2 THE CASE STUDY

We consider a simply supported RC beam externally strengthened with two symmetrically bolted side plates exposed to mechanical and thermal loads simulating ISO 834 fire conditions. The geometrical, loading, and reinforcement data of the problem along with its hygro-thermal boundary conditions are presented in Fig. 2. The initial relative humidity of air inside the concrete pores is chosen as 60% and the surrounding air relative humidity is 40%. Furthermore, initial porosity of concrete is set to $p_{or,0}$=0.12 and the initial permeability in the top surface of the concrete section is $k_{top}=3\cdot10^{-15}$m^2. The side plate and the beam are connected by 2 parallel rows of 8 (case 'c1') or 5 (case 'c2') bolts at each end and each side of the beam. For each of the connectors the constitutive law of contact as suggested by Huang et al. (1999) is used, where for the maximal bearing capacity of a shear connector at room temperature P_{max}=40kN is chosen. The material data at ambient temperature used in the analyses are: compressive strength of concrete $f_{c,20}$ = 3.43kN/cm^2, elastic modulus of concrete $E_{c,20}$ = 3250kN/cm^2, yield strength of steel $f_{ys,20}$ = 33.5kN/cm^2, elastic modulus of steel $E_{ys,20}$ = 21200kN/cm^2, yield strength of reinforcing steel $f_{ya,20}$ = 53.7kN/cm^2, and elastic modulus of reinforcing steel $E_{ya,20}$ = 18700kN/cm^2. In the analysis, the fire response of the both beams (cases 'c1' and 'c2') will be compared against the response of the unstrengthened beam (case 'c3') and further against each other.

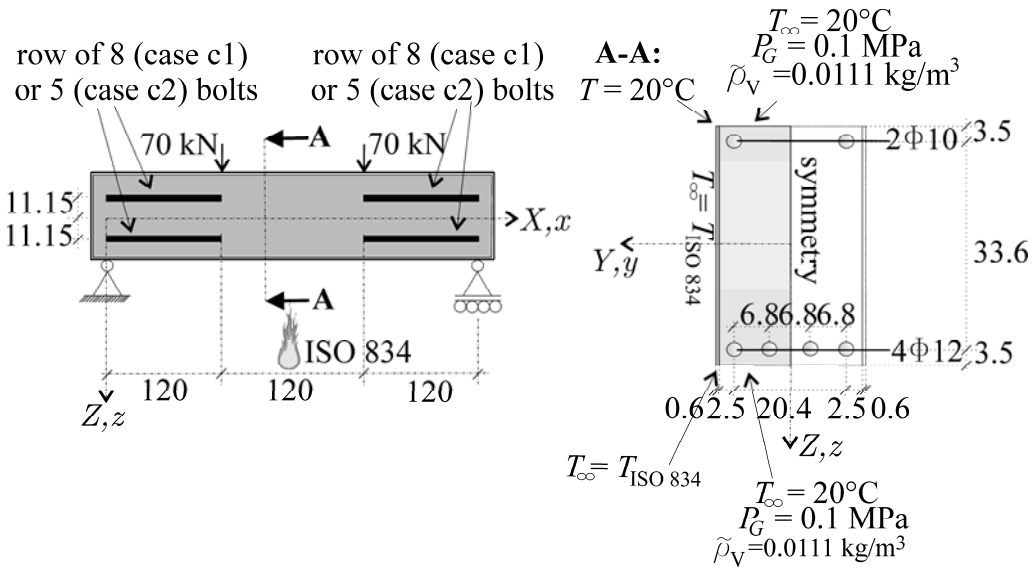

Fig. 1: Geometrical data, loading data, reinforcement data and the hygro-thermal boundary conditions.

The distributions of temperature and pore pressures over the concrete part of the cross section of the side-plated beam and over the cross section of the unstrengthened beam at 22 and 45 min are shown in Fig. 3a. The effect of the vapour-tight side plate preventing the vapour from escaping the side-plated beam is here seen clearly. In comparison to the unstrengthened beam, increased pore pressures are observed along the steel–concrete contact in the side-plated beam resulting in a slight reduction of temperatures of concrete (observe the hottest regions of the cross-section). Nevertheless, the rate of pore pressures evolved in concrete is small in both cases, therefore, their contribution to the total stress of the RC beam can be neglected from the proceeding mechanical subanalysis. Moreover, as confirmed by the criterion of concrete spalling, suggested by Dwaikat and Kodur (2010), in the presented cases spalling of concrete is only superficial and can be also neglected. As in the present analysis characteristics of normal strength concrete have been assumed, such conclusions are rather expected.

Fig. 4 shows the increase of the midspan deflection with time for the two observed cases ‘c1’ and ‘c2’. The bearing capacity of the strengthened beams ($t_{cr} \approx 45$ min) is here obviously greater than that of the unstrengthened beam ($t_{cr} = 23$ min) and almost a 100% increase in the fire resistance of the RC beam after its strengthening is observed. By comparing the results for the side–plated beams ‘c1’ and ‘c2’, however, higher number of bolts would appear unreasonable at first glance, especially since for both cases load-deflection curves as well as the predicted fire resistances (t_{cr}) are almost identical. Nevertheless, as observed in the numerical analysis, by increasing the number of bolts (case ‘c1’), the pronounced creep deformations in the reinforcement bars of the RC beam would be discovered prior to the collapse and a material instability of the concrete part of the composite cross-section would be eventually reported. Because, in this way, the structure would not fail due to a contact failure (as it would in the alternative case of the ‘c2’ beam) the bearing capacity of the beam would be fully exploited. In contrast to the case shown in this paper, this could be of a special importance, if the RC beam was sufficiently strong.

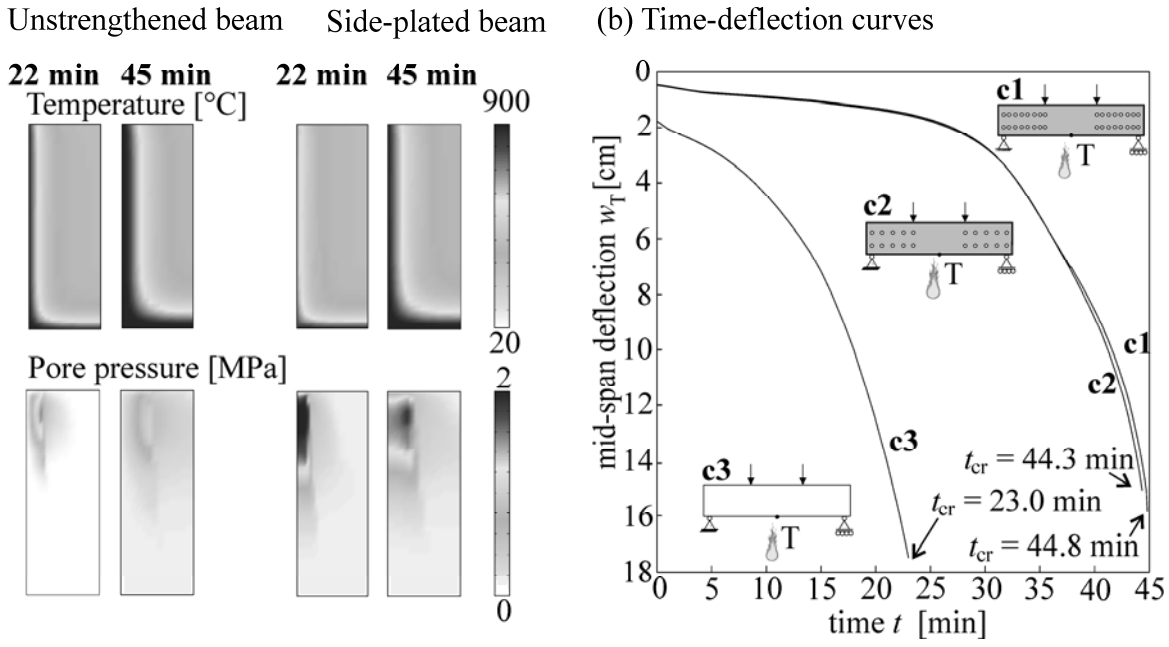

Fig. 2: (a) Temperature and pore pressure distributions in the mid-span cross-section of the analysed beams. (b) The time-deflection curves.

REFERENCES

Davie C.T., Pearce C.J., Bićanić N., Coupled heat and moisture transport in concrete at elevated temperatures - Effects of capillary pressure and adsorbed water. Numerical Heat Transfer, Part A: Applications 49 (2006) 733 – 763.

Dwaikat M. B., Kodur V. K. R., Fire induced spalling in high strength concrete beams. Fire Technology 46 (2010) 251 – 274.

Gawin D., Pesavento F., Schrefler B.A. Simulation of damage-permeability coupling in hygrothermo-mechanical analysis of concrete at high temperature. Communications in Numerical Methods in Engineering 18 (2002) 113 – 119.

Gawin D., Pesavento F., Schrefler B.A. Modelling of hygro-thermal behaviour of concrete at high temperature with thermo-chemical and mechanical material degradation. Computational Methods in Applied Mechanics and Engineering 192 (2003) 1731 – 1771.

Hozjan T., Saje M., Srpčič S., Planinc I. Fire analysis of steel-concrete composite beam with interlayer slip. Computers and Structures 89 (2011) 189-200.

Huang Z., Burgess I., Plank R. The influence of shear connectors on the behaviour of composite steel-framed buildings in fire. Journal of Constructional Steel Research 51 (1999) 219 – 237.

Kolšek J. Fire analysis of two-layered composite structures, University of Ljubljana, Faculty of Civil and Geodetic Engineering, Doctoral thesis (in Slovene), 2013.